Journal of Materials Chemistry A

COMMUNICATION

View Article Online
View Journal | View Issue

Cite this: J. Mater. Chem. A, 2019, 7, 17806

Received 16th April 2019
Accepted 3rd July 2019

DOI: 10.1039/c9ta03990b

rsc.li/materials-a

High density assembly of energetic molecules under the constraint of defected 2D materials†

Qi-Long Yan, *[a] Zhijian Yang,[b] Xue-Xue Zhang,[a] Jie-Yao Lyu,[a] Wei He,[a] Shi Huang,[b] Pei-Jin Liu,[a] Chaoyang Zhang,[b] Qing-Hua Zhang,[b] Guo-Qiang He[a] and Fu-De Nie[b]

High energy density is always a key goal in the development of energy storage or energetic materials (EMs). Apart from exploring novel EMs with high chemical energy, it is also desirable for traditional EMs to be assembled at a higher density. It has been shown that a molecular level compression effect occurs due to the stacking of 2D triaminoguanidine–glyoxal polymer (TAGP) layers, resulting in a higher density packing of HMX molecules with changed conformation (qy-HMX). The qy-HMX crystal formed under compression in the solvent has a unit cell parameter very close to that of a reported system observed under a pressure of 0.2 GPa. This shows that the qy-HMX molecules are trapped in the TAGP layers, resulting in a higher density (*e.g.* 2.13 g cm^{-3}), heat of formation and better stability. Certain types of constrained qy-HMX crystals are free from defects, where no polymorphic transition and melting point are observed upon heating. Experiments and relevant calculations show that the best resulted hybrid HMX crystal has a detonation velocity of 10.40 km s^{-1} and pressure of 53.9 GPa, respectively. Its ground specific impulse reaches about 292 s, much better than that of CL-20, making it a promising propellant component for use in future space explorations.

It is essential to develop energy storage or energetic materials (EMs) with higher energy densities. In recently years, more and more attention has been paid to this field, due to the high demands of deep-space exploration, aerospace and defense technologies. Typical novel highly EMs include energetic ionic liquids,[1] metastable intermixed composites (MICs),[2] novel insensitive nitro-compounds,[3] full nitrogen compounds,[4,5] polynitrogen compounds,[6] boron–nitrogen based EMs,[7] as well as carbon nanomaterial-based energetic nanocomposites.[8] However, most of these newly developed high EMs are still not qualified to replace currently used EMs due to various problems, including chemical incompatibility, thermal instability, high sensitivity, as well as high cost. Another group of fancy disruptive EMs are so-called extended solids, with typical representatives of these being metallic hydrogen[9] and poly-CO.[10] Solid molecular hydrogen under an extremely high pressure (*e.g.* >495 gigapascals) is metallic with a reflectivity of over 0.9, which is considered to be a room-temperature superconductor and very promising for use as a rocket fuel if it could be stabilized under mild conditions. However, these materials are only stable under extreme conditions. Theoretically, they are revolutionary in terms of structure and performances, but much more effort still has to be made before their practical applications.

Despite great progress in the development of novel EMs, the widely used energetic ingredients in formulations are dominated by 1,3,5-trinitro-1,3,5-triazinane (RDX), 1,3,5-triamino-2,4,6-trinitrobenzene (TATB), 1,3,5,7-tetranitro-1,3,5,7-tetrazocane (HMX), hexanitrohexaazaisowurtzitane (CL-20) and aluminum (Al).[11] For enhanced performances, these conventional EM materials have to be modified by new processing technologies.[12] Much research work has been done on this issue over the past decades, where successful strategies have included particle polishing,[13] coating,[14] co-crystallization,[15] and doping with 2D materials such as graphene.[16] In the case of coating and doping strategies, polydopamine[17] and graphene oxide[18] have been widely used to improve the safety of energetic composites[19] or energetic crystals.[20] To improve the homogeneity and safety of energetic composites, some advanced fabrication techniques may also be implemented, including vapor deposition[21] and electrospinning methods.[22]

Alternatively, if the abovementioned energetic molecules or fuels could be packed at a higher density during modification, it would be highly desirable, since the performances of these materials are largely dependent on their density. However, it is very difficult to surpass their theoretical maximum density

[a]Science and Technology on Combustion, Internal Flow and Thermo-structure Laboratory, Northwestern Polytechnical University, Xi'an 710072, China. E-mail: qilongyan@nwpu.edu.cn

[b]Institute of Chemical Materials, CAEP, Mianyang, 621900, China

† Electronic supplementary information (ESI) available: Supporting Information includes the following content: Materials and methods; Fig. S1 to S17; Tables S1 to S14; (ref. S1–S8). CCDC 1850522–1850523. For ESI and crystallographic data in CIF or other electronic format see DOI: 10.1039/c9ta03990b

under ambient conditions, even though a higher molecular density packing could be achieved due to conformation changes of the component molecules under ultra-high pressure (gigapascals, usually using a diamond anvil).[23] It has been demonstrated that such solid-state phase changes are reversible, and hence this high density packing is not able to be maintained under ambient conditions.

With the aim of achieving irreversible high density packing, molecular level *in situ* compression of energetic molecules during their crystallization in solutions would be an appropriate choice. However, there are few chemical reactors that can reach pressurization of over a gigapascal due to limited sealing technology and material strength. Interestingly, we found that a molecular level compression effect could be achieved between layers of 2D materials during their stacking at a high temperature (~150 °C), resulting in a large conformational change in energetic molecules trapped between these layers. This 2D material was actually recently reported, which has large hollow defects on its layered structure.[24] It is an analogue of graphitic carbon nitrite (g-C_3N_4) named TAGP (triaminoguanidine–glyoxal polymer).

To symbolically depict this compression and the following molecular packing process, herein the term "net-fishing" has been selected to give a vivid description. As a demonstration, highly energetic nitramine HMX molecules were used for this research, and the corresponding reaction scheme is presented in Fig. 1A. The dragging force of the "net-fishing" process is the strong interaction of π–π stacking among the *in situ* generated TAGP networks in concentrated dimethylsulfoxide (DMSO) solution, and the preconditions for squeezing the DMSO molecules out is the absorption force of water as the anti-solvent and large hollow defects present on the TAGP layers, which act as the "fishing net". Such a stacked 2D network has a size of one or two nanometers, so that it is difficult for the large HMX molecules to travel through as the trapped "big fishes", whereas the solvent DMSO molecules are squeezed out (Fig. 1C). Also, the hydrogen bonds between the –NO_2 group and –NH– on the TAGP skeleton is another force that prevents HMX molecules from being expelled. It has been found that a large variety of doped/modified qy-HMX crystals can be obtained under different experimental conditions. This is a very facile and flexible method combining *in situ* cross-linking and co-crystallization techniques, where the insensitive high-nitrogen 2D TAGP networks can be integrated or doped in HMX crystals *via* a constraining force. The TAGP layers play a dual role as both compressing "anvils" and dopants, so that various hybrid energetic crystals with different structures and densities were obtained, depending on the experimental conditions (details of the experiments and nomenclature of the typical products are presented in the ESI†). Typical selected products with different colors are shown in Fig. 1B and S1.†

As shown in Fig. S1,† cream white industrial grade β-HMX was transformed into various colors, including yellows, grey, dark brown and black due to the change in compositions, crystal structures, and molecular conformation after doping of the TAGP network. In order to compare the crystal morphologies of these products, the scanning electron microscopy (SEM) images (Fig. 2A–G and S2†) coupled with elemental analyses by EDS (Fig. $2p_1$–p_4 and S3†), as well as transmission electron microscopy (TEM) images (Fig. 2H–L) were obtained. As shown in these figures, it is clear that the qy-HMX crystals obtained under different conditions show very different morphologies. In general, the shapes of these HMX crystals can be simply divided into three categories: polyhedral (Fig. 2A and E), stick (Fig. 2B and C), and flake (Fig. 2D, F, and G). It is clear that the slow growth of crystals H-1 and H-4 resulted in the formation of very different morphologies to those of their counterparts obtained by fast crystallization. However, in the case of HT-7, both fast and slow crystallization led to the same flake structure, where the only difference is the dimensions (aggregations of tiny flakes *vs.* large plates of hundreds of microns in size). This means that at a higher temperature, a larger TAGP network could be formed with less defects, and under the guidance of these layers, the crystal could be inclined to grow in 2D pattern.

As a common fact, nitramine crystals are very sensitive to the electron beam used in SEM and TEM techniques. TEM images were obtained by measurements on the filtrated precipitates after dissolving of the corresponding qy-HMX crystals, mainly the TAGP dopants. However, it is clear that some blocks of tiny HMX crystals were still trapped inside the layers of TAGP and did not dissolve (Fig. 2I, J and S18†). It is clear from the presented SEM (Fig. 2F) and TEM (Fig. 2I) images that some black spots are present on the surfaces of the involved crystals after short-exposure to the electron beam, even at a lower voltage of 5 kV, where HT-0, HT-1, HT-2 and HT-4 are even more sensitive than the others. The nontransparent blocks shown in Fig. 2I and J are the carbonized remnant HMX crystals after exposure to a high voltage electron beam.[25] Typically, there are two types of 2D TAGP materials formed in the mother DMSO solution. One is curly and round-packed layers of TAGP with large hollow defects that look like a fishing-net (Fig. 2H). Another is a smooth transparent graphene-like film without any defects. In the presence of highly concentrated HMX molecules, a part of the original defected TAGP skeleton could be repaired. As a demonstration, after dissolving of the crystals of HT-1, HY-4 and HT-7 in a mixed solvent of acetone and ethyl acetate, the doped TAGP materials could be separated by simple evaporation of about 1/3 of the saturated solution. The materials are very different in morphology: the TAGP inside HT-1 is a mixture of nanofibers and thin film (Fig. 2J), and it is a hollow thin film in HT-4 (Fig. 2K), whereas defect free 2D layers are presented in the HT-7 crystals (Fig. 2L).

HMX is a flexible eight-membered ring compound and can exist in different conformations, leading to different crystal structures with different thermal stability, sensitivity, and reactivity. These crystals are named as α-, β-, γ- and δ- polymorphs.[26] β-HMX is the most stable and is widely used in various applications. In the beginning, we believed that these crystals were hybrid crystalline materials (multi-phase, dopants with various molecular weights), and it was very difficult to analyze their structures using single-crystal X-ray diffraction. Therefore, to clarify their structural discrepancies, aside from mass spectrometry and NMR spectroscopy (Fig. 3A, and S6, S7

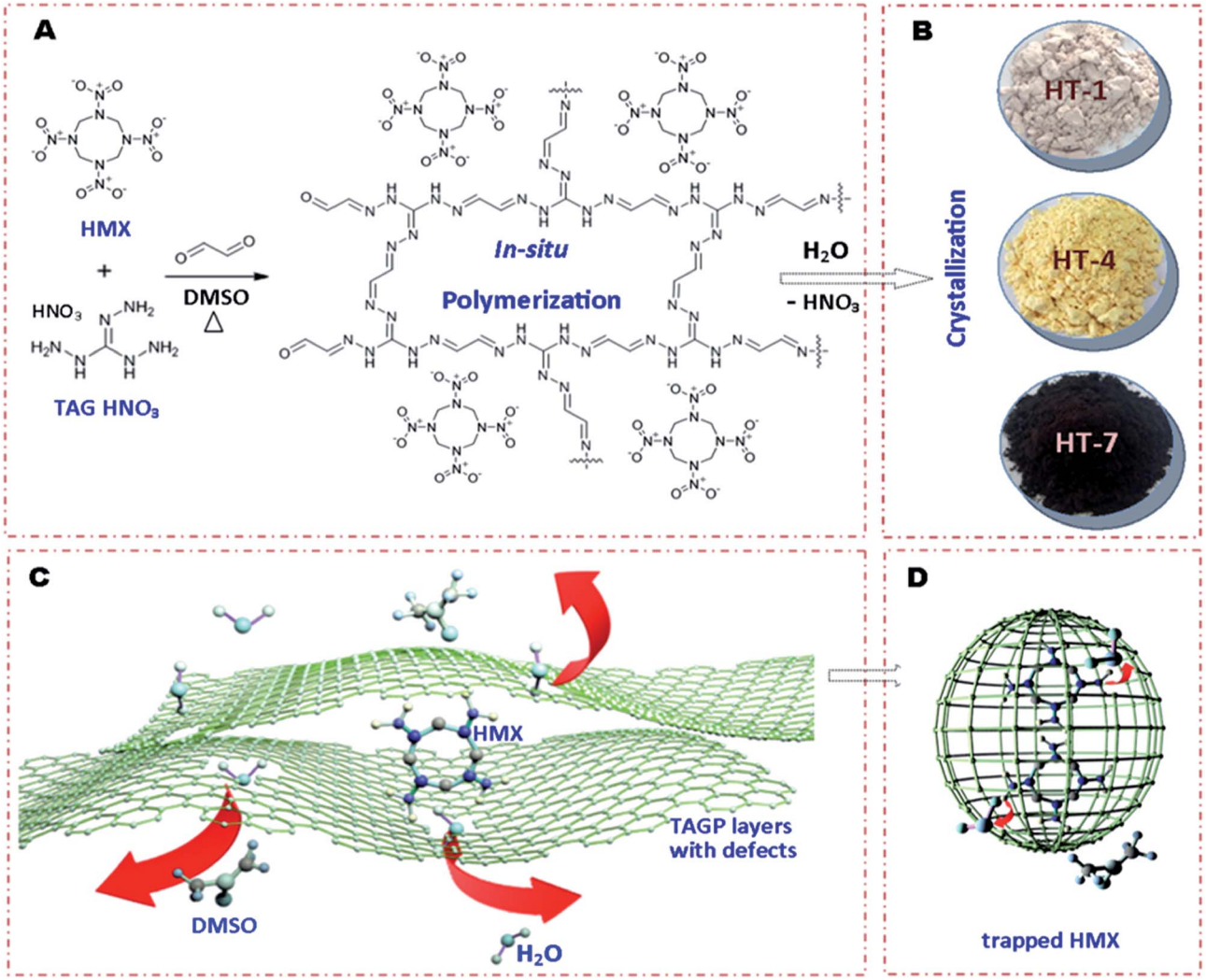

Fig. 1 The reaction mechanisms and proposed concept of "net-fishing": (A), the chemical reaction mechanism of triaminoguanidine nitrate with glyoxal in the presence of dissolved β-HMX in DMSO. (B) Digital photos of typical as-prepared products: crystalline powders of HT-1, HT-4 and HT-7 (DMSO/H_2O solvent/anti-solvent system). (C) Scheme of the packing and squeezing process of the DMSO molecules from HMX aggregations by 2D TAGP stacked layers with hollow defects, which is therefore vividly so-called a "net-fishing" process. (D) The trapped HMX molecules crystalize in enclosed TAGP layers as the dopants, as shown in Fig. 2H.

and S12†), various popular techniques used in materials science were attempted, including FTIR (Fig. S4†), Raman (Fig. S5†), XPS (Fig. 3B, C, S10 and S11†), powder XRD (Fig. 4C, S8 and S9†) and small-angle X-ray scattering (SAXS) analyses (Fig. 4A and B).

It is clear from the MS, FTIR and NMR spectra that these techniques do show us some difference between the pristine HMX and the modified/doped HMX crystals, and one thing that can be confirmed is that the HMX molecules did not decompose during crystallization under constraint. The Raman spectra are greatly dependent on the capability of the light scattering used for the samples, therefore the crystals that are deep in color (*e.g.* dark brown HT-3 and black HT-7, see Fig. S1†) have fewer peaks or broader peaks. As reported in the literature, HMX displays a fingerprint-like quality for β-HMX in the region of 200–600 cm^{-1}, whereas peaks in the 800–960 cm^{-1} and 1000 to 1500 cm^{-1} region are attributed to the ring-stretching vibration and symmetric vibrational stretching of the NO_2 and N–NO_2 groups of the HMX molecules, respectively. Only HT-7 does not show these typical peaks due to very weak light scattering, which contains the highest mass ratio of TAGP dopant among all of the prepared samples (about 24.67%), whereas HT-4 contains a TAGP content of about 1.96 wt%, as determined by gel permeation chromatography (GPC) (Fig. S13†).

The deconvolution of the XPS spectra (Fig. S10 and S11†) and elemental analyses (see in Fig. S3, S4 and Table S1†) show the successful doping of the TAGP materials inside the HMX crystals. The presence of C–C and N–H bonds, with binding energies of about 283.4 and 398.3 eV, respectively, confirm the presence of $-[NH-N-C(=N-N-)-N-NH-C-C]_n-$ networks (Fig. 1A) inside the modified HMX crystals. The elemental analyses using combustion shows that after doping, there is about a 0.06–0.13 wt% increase in the C content and 0.09–0.20 wt% increase in the O content, whereas the N content decreases by 0.22–0.24 wt% with the hydrogen content almost

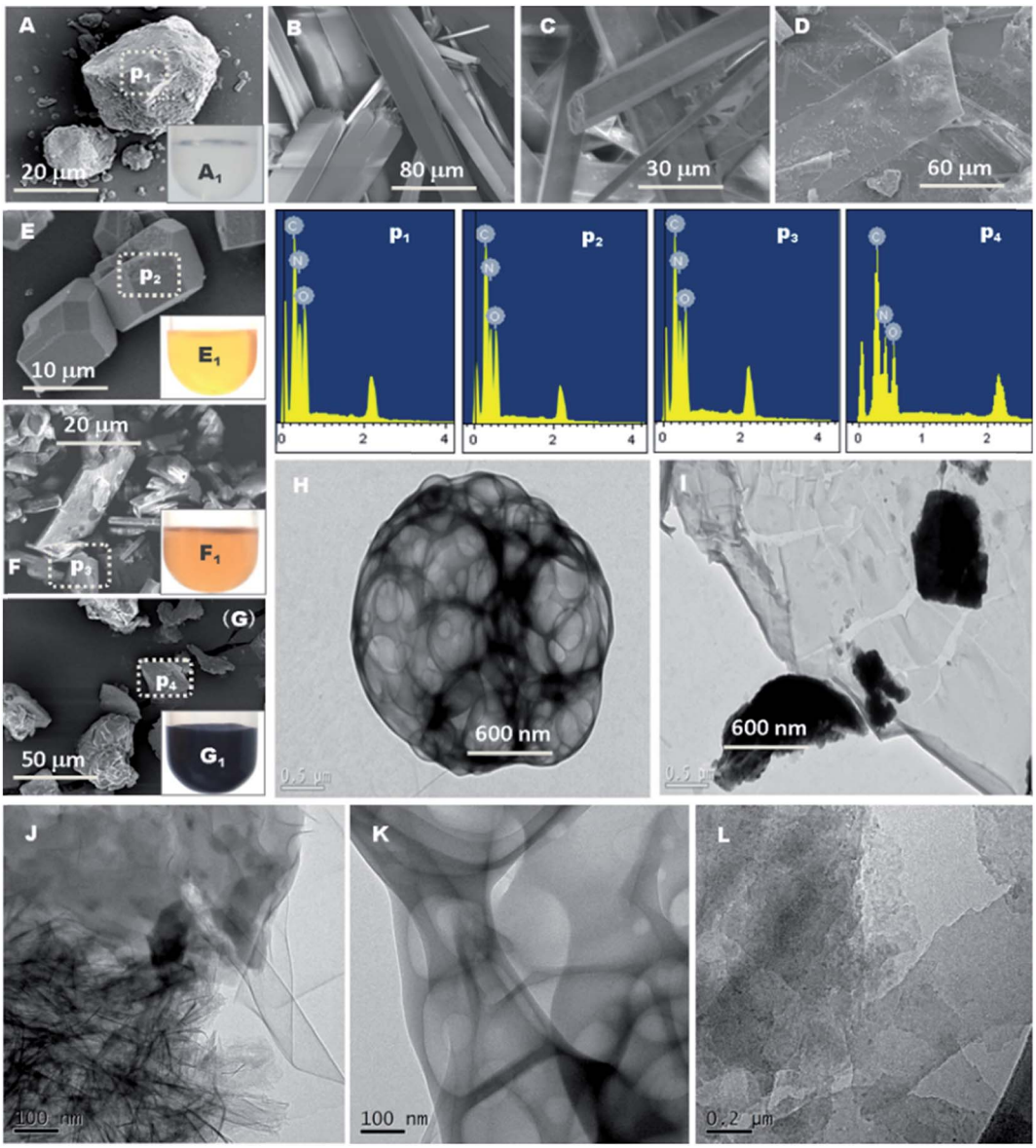

Fig. 2 The SEM/EDS and TEM images. (A) The SEM images of pristine β-HMX as the starting material. (B–D), SEM images of the HT-1, HT-4 and HT-7 crystals obtained *via* a slow crystallization process (DMSO/H_2O solvent/anti-solvent system, diffusing and dissolving for over one month in DMSO at room temperature). (E–G) SEM images of the HT-1, HT-4 and HT-7 crystals obtained *via* a slow crystallization process (DMSO/H_2O system, water added in 10 minutes). (H and I) TEM images of nanomaterials that disperse in DMSO/H_2O solutions after the crystallization process of HT-4 and HT-7, respectively. (J–L) TEM images of the separated dopants after slow half evaporation of saturated solutions of the HT-1, HT-4 and HT-7 crystals using acetone/ethyl acetate in a 1/1 volumetric ratio. (A_1), (E_1), (F_1) and (G_1), the appearance of the DMSO saturated solutions of β-HMX, HT-1, HT-4 and HT-7 at room temperature, respectively. (P_1–P_4) EDS spectra of the marked areas in the corresponding SEM images.

unchanged. In order for better comparison, these changes are based on the measured elemental content of HMX as the starting reference material. The measured O content of HMX is about 1.43 wt% higher than the theoretical value, whereas the other elements are lower. Since the TAGP dopants are different in size (due to extent of crosslinking) and structure due to different reaction conditions, as shown by TEM, we could not simply use a single formula to represent these TAGP.

For better comparison, the experimentally measured formula with normalized number of carbon atoms for the modified HMX and raw β-HMX crystals are presented in Table S1.† However, such a small change in elements after TAGP doping resulted in large differences in the crystal structure and density. According to the SAXS results shown in Fig. 4A and B, we obtained the phase dimensions of the pure HMX crystal and hybrid crystals of qy-HMX (HT-4 and HT-7), which is connected to the level of doping. Guinier analysis (Fig. 4A, when q is very small) provides important information about sample aggregation and interparticle interference. An increase in the concentration of TAGP dopant greatly affects the value of log (I_0) due to changes in interparticle repulsion. There are single peaks with almost the same maximum value of scattering vector $\boldsymbol{q}$ located

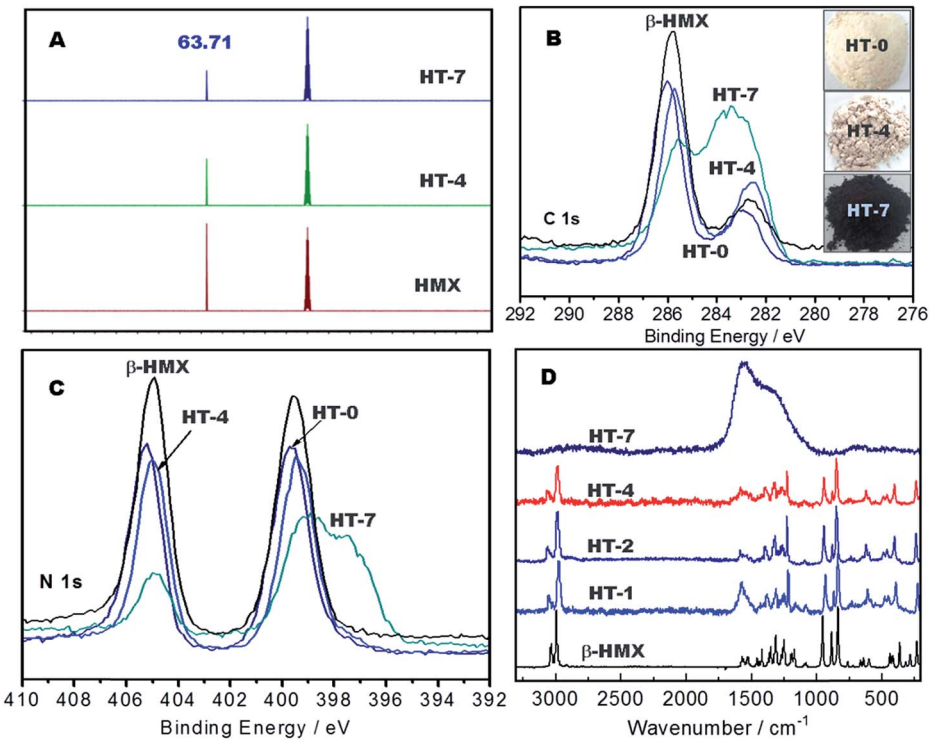

Fig. 3 The atomic and molecular spectrometry. (A) The ^{13}C NMR spectra of the starting material HMX, products HT-4 and HT-7. (B and C) The C 1s and N 1s XPS spectra of the β-HMX, as-prepared HT-0, HT-4 and HT-7 crystalline powders, respectively. (D) Raman spectra of the β-HMX, and HT-1, HT-2, HT-4 and HT-7 crystals powders, where only the black sample H-7 shows a broad peak, due to a high absorption coefficient.

at 0.09 nm^{-1}. The sharp peaks indicate that both HMX and qy-HMX are fully crystalline. As shown in Fig. 4B, the pair distance or vector length distance function $P(r)$ distribution is related to the position of electrons within the scattering samples.[27] When samples are aggregated, the $P(r)$ distribution does not approach zero in a smooth way. The D_{max} value represents the longest linear distance across a qy-HMX crystal, or, in simpler terms, the maximum width of the crystals. With the TAGP layers doped inside the HMX crystals, two shoulder peaks could be observed above the D_{max} of HMX at about 28 nm. These can be attributed to the scattering from the TAGP dopants dispersed in the crystals of HT-4 and HT-7, where the latter has a higher concentration of TAGP, resulting in a larger D_{max} value. Moreover, the general overall structure of a protein can be determined by the shape of the $P(r)$ distribution. This indicates that HT-7 is a flat disk, whereas HT-4 and pure HMX are solid spheres, according to the reference curves,[28] which is in agreement with the SEM results (Fig. 2).

Moreover, the powder X-ray (PXRD) spectra (Fig. 4C) show that at least HT-1, HT-2, HT-4 and HT-7 do not belong to any form of polymorphs of existing HMX or their mixtures, showing extra peaks (*e.g.* 18.6°, 34.1°) or shifted peaks at various diffraction angles (Fig. S8 and S9†). The calculated space groups from the PXRD patterns for these modified HMX are quite different from the existing polymorphs of HMX, except for HT-0, HT-5 and HT-8 (Table S2†), which show almost identical PXRD patterns to those of β-HMX (Fig. S8†). This means that the TAGP material is not well assembled with the HMX molecules, resulting in a decreased density. The other qy-HMX crystals with a different crystal structure have a higher density than pristine β-HMX, where HT-7 has the highest density of 2.13 g cm^{-3}.

As mentioned earlier in this work, if we dissolve the qy-HMX powder with a higher density, the solutions are homogenous with a different color (Fig. 2), from which slow recrystallization could be achieved. For instance, powdered qy-HMX with TAGP dopants and pristine β-HMX were recrystallized naturally by slow dissolving of these materials in DMSO solutions with ethanol as the anti-solvent. It is easy to grow micron-sized qy-HMX crystals, but these crystals are not as homogenous as their as-prepared powdered counterparts due to the random doping of TAGP layers with different sizes during the slow crystallization process, resulting in a discontinuous color (Fig. 5A1–A3). In this case, it is extremely difficult to clarify how these TAGP layers are intercalated in the crystals of these composite HMX-based crystals. Interestingly, if we separate the dopant TAGP layers and the HMX molecules using a mixture of acetone and ethyl acetate as the solvent, based on which the crystals of squeezed HMX (qy-HMX) molecules can be obtained, the structure can be determined (CCDC 1850523†) by single-crystal X-ray diffraction. The qy-HMX crystal obtained from HT-4 and HT-7 shows almost the same cell parameters, but a higher crystal density than that of the original β-HMX (Table S4†). This means that even after removal of the dopants, the modified HMX molecules assemble with a higher density due to permanent conformational change upon compression of the 2D TAGP material.

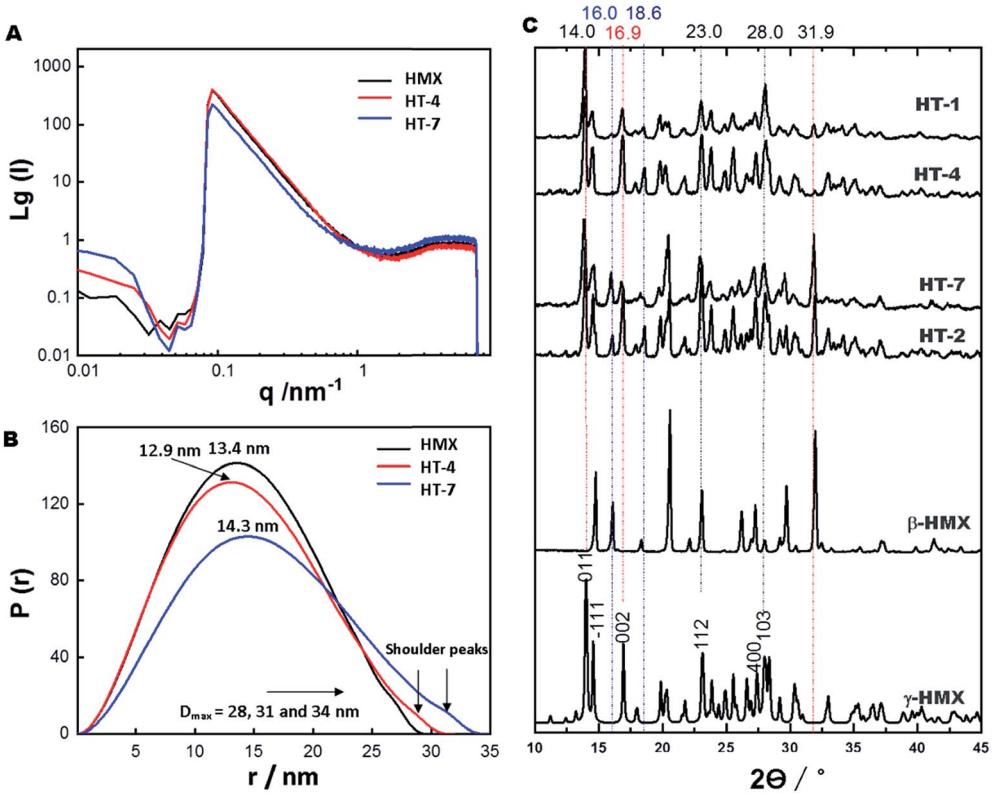

Fig. 4 (A) The dependence of the scattering intensity, $I(q)$, as a function of the scattering vector q; (B) pair distribution functions, $P(r)$, related to the position of electrons within the scattering qy-HMX samples from small-angle X-ray scattering (SAXS); (C) powder X-ray spectra of β-HMX, γ-HMX, and the as-prepared HT-1, HT-4, HT-7 crystals.

The crystal lattice unit cell parameters of qy-HMX are as follows: monoclinic, space group $P2_1/c$ (no. 14), with a = 6.527(5) Å, b = 10.926(7) Å, c = 8.699(7) Å, β = 124.59(2)°, V = 510.6(7) Å^3, $Z = 2$, $D_{calc} = 1.926$ g cm^{-3}. The conformation of the squeezed HMX molecules and the resulting qy-HMX crystal is very close to that of β-HMX when it was hydrostatically pressed at a pressure of 0.2 GPa, named as HMX-II.[17] The refined cell parameters of HMX-II are as follows: space group $P2_1/c$, a = 6.495(±0.014) Å, b = 10.952(±0.010) Å, c = 8.693(±0.024) Å, β = 124.53(±0.20), D_{calc} = 1.931 g cm^{-3}. These pressed/squeezed structures are both consistent and proportional to those of β-HMX under ambient conditions: a = 6.54 Å, b = 11.05 Å, c = 8.70 Å, β = 124.30°, D_{calc} = 1.893 g cm^{-3}.[28]

The same single-crystal X-ray experiment was carried out on squeezed RDX, but little change was observed for its conformation (CCDC 1850522†), even though the corresponding doped RDX crystal has a density of 2.04 g cm^{-3}. This means that the doping method of TAGP with constraining effect is universal, but that the extent of conformational change greatly depends on the rigidity of the molecules, since the HMX molecules with an eight-membered ring are much more flexible than RDX. This reveals that after squeezing by the TAGP layers, the conformation of HMX was largely changed (Tables S5–S10 and Fig. S16†). DFT calculations using the experimental CIF file (CCDC 1850523†) of pure qy-HMX show that it is a completely new crystal phase of HMX. Its stability is even better than the most stable form (β-HMX) as reported. In the presence of solvent molecules (liquid state), such change is irreversible, and hence the new conformation was maintained during the recrystallization process even after removal of the dopants, resulting in a higher packing density (Table S4 and Fig. S16†).

Polymorphic HMX crystals form due to different arrangements of molecules in the unit cells, and thus display very different solid-state properties, such as density, thermodynamic and physicochemical properties, including dissolution rate, stability, hardness, and spectroscopic properties. These properties are strongly related to their product quality and performance. As the most stable form at room temperature, β-HMX is stable below the temperature of 185 °C,[29] after which a polymorphic transition β → δ occurs, showing the first endothermic peak at 190.5 °C (Fig. 5A) and followed by partial melting with a peak temperature of 280.1 °C before decomposition. It has been reported that under a pressure of over 0.12 GPa, such transition was excluded and HMX decomposes in the state of the β-form.[17] Interestingly, it is also the case for HT-1, H-4 and HT-7, where no endothermic peak was shown before their decomposition. More importantly, the thermal stability has been improved in the cases of HT-1 and HT-4. This means that after squeezing of the TAGP layers as dopants, the HMX molecules with modified conformation and extra constraining force are no longer sensitive to the temperature. In addition, interestingly, there is no heat change in the

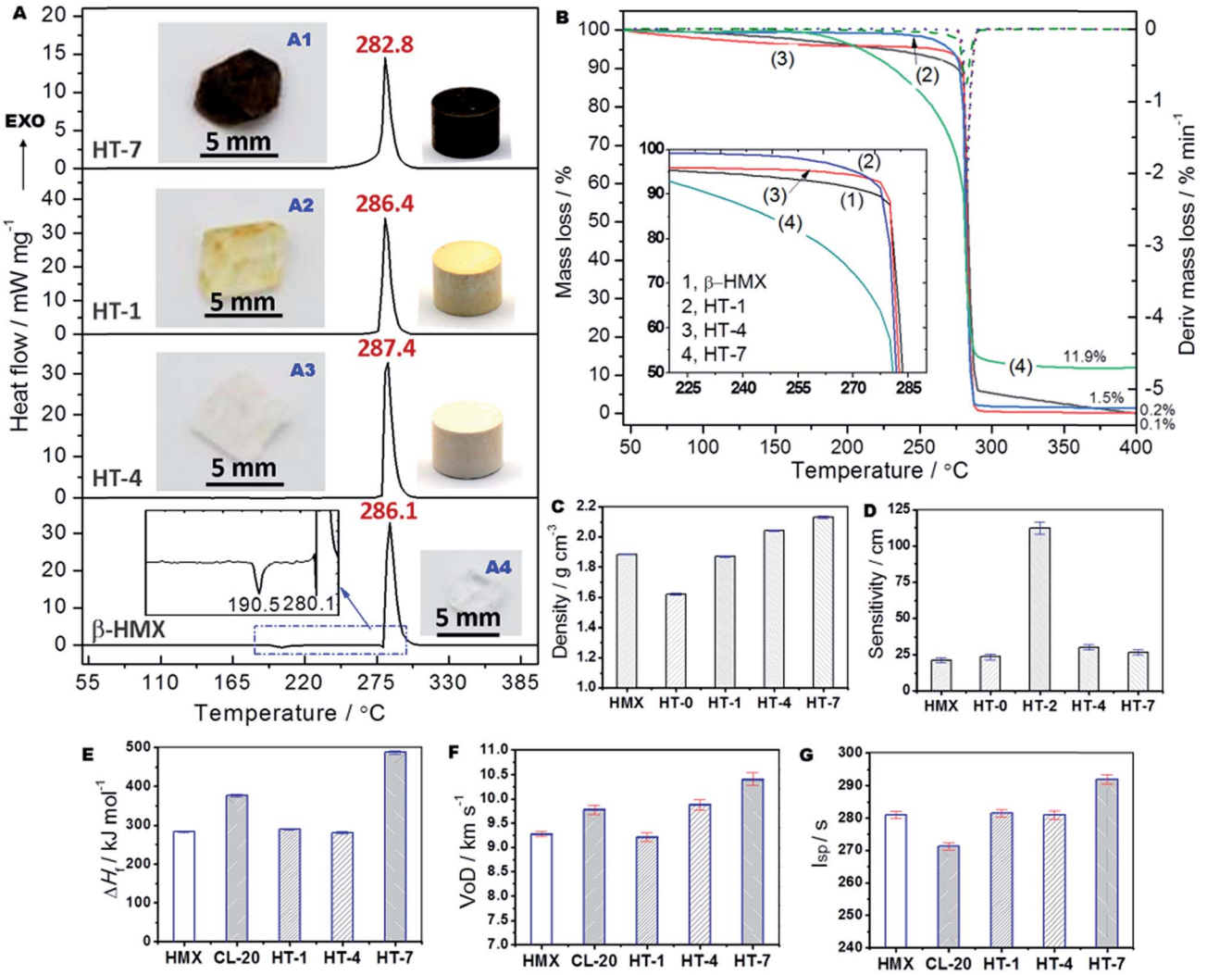

Fig. 5 Thermal behavior, density, safety and performances. (A and B) Non-isothermal DSC and TG curves of the starting material β-HMX and products HT-1, HT-4 and HT-7 with a heating rate of 10 K min^{-1}, where the products show no endothermic peaks due to exclusion of the polymorphic transition and they have obvious different mass loss behavior due to the variation in doping content. (A1–A4) Digital photos of the selected micron-sized modified HMX crystals; (C), comparison of the crystal density measured by densitometer using helium as the filling gas. (D) The impact sensitivity (energy) of raw HMX and the selected modified HMX, evaluated using a 5 kg dropping hammer according to the military standard documented as GJB 772.206–1989. (E–G) Experimental heat of formation (ΔH_f), calculated detonation velocity (VoD) and specific impulse (I_{sp}) of raw β-HMX and typical TAGP doped HMX crystals under identical conditions.

temperature range of 180–220 °C (Fig. 5A, Tables S12 and S14†), which is supposed to be when the exothermic decomposition of the TAGP layers occurs.[24] This further indicates the successful intercalation of these 2D materials in the crystal of HMX, and therefore the hybrid crystal lattice stabilizes the TAGP structure, resulting in a complex single exothermic peak.

In terms of the decomposition heat under the same experimental conditions, the heat of TAGP-doped HMX is higher than that of pristine HMX (1574 J g^{-1}), except for HT-7, and the highest heat produced by HT-2 is about 1688 J g^{-1}. More importantly, HT-2 is also the safest material out of all of the presented samples, with an impact sensitivity (I_m) of 112 cm (54.9 J, Fig. 5D), whereas it is 24 cm (11.8 J) in the case of pristine HMX. One has to note that these I_m values are obtained based on the Chinese military standard, which is usually over two times greater than that of the BAM standard. As shown in Table S14,† the densities of HT-4 and HT-7 are around 2.04 and 2.13 g cm^{-3}, respectively, even higher than that of the currently used most powerful explosive ε-CL-20. In comparison, HT-0 has the lowest density of 1.62 g cm^{-3}, which is much lower than that of pristine HMX and even close to that of the TAGP material (1.54 g cm^{-3}). This means that the intercalation of TAGP under different experimental conditions results in various states of molecular assembly with different packing densities, which makes the performances of the doped energetic crystals tunable. One can also notice that the decomposition residues of HT-0 and HT-7 (Table S12†) are much higher than those of the other materials, due to the nonvolatile products from the higher content of TAGP dopant. It has been reported that TAGP decomposes with a residue of about 45.4 wt%,[24] and herein, HT-

7 contains about 24.67 wt% TAGP, resulting in a residue of 11.9 wt% (Fig. S15,† 45.7% × 24.67% = 11.2%), which further validates the GPC results (Fig. S13†).

In order to compare the performances of these new EMs, as routine work, the heat of formation was calculated based on the experimental heat of combustion data. Then, the detonation velocity (VoD) and ground specific impulse (I_{sp}) were calculated using commercial code "Explo-5" based on the experimental data: density, heat of formation (ΔH_f), as well as elemental content. For better comparison, pristine HMX as a starting material was also measured in all cases, resulting in slightly different formulae (Table S14†). The heat of combustion values (ΔH_c) vary a lot, and the ΔH_c per unit mass values are all increased after doping, but the ΔH_f values of β-HMX, HT-0, HT-1 and HT-4 do not differ too much due to the corresponding changes in elemental content (Fig. 5E). Even using the experimental formula, the obtained VoD value of pristine β-HMX (9277 m s^{-1}) is very close to the average value of the reported VoD using its theoretical formula. It has been shown that the heat of combustion (ΔH_c) of the doped HMX is higher than that of pristine HMX, especially in the case of HT-7, the ΔH_c value of which is as high as 10.36 kJ g^{-1}. As a common fact, the performances of EMs are highly dependent on their density, especially in the case of detonation pressure ($P_{C\text{-}J}$). One could notice that HT-7 reaches a $P_{C\text{-}J}$ of 53.87 GPa (Table S14†), which is 35% higher than that of the pristine HMX, even higher than the most powerful energetic compound ε-CL-20 (44.98 GPa) currently in service. In terms of VoD and I_{sp}, the values of HT-4 and HT-7 are both higher than those of pristine HMX and even ε-CL-20 (Fig. 5F and G). In particular, the calculated values of VoD for HT-7 and HT-4 are 10.40 and 9.88 km s^{-1}, respectively, indicating that these materials could be widely used in both military and civil applications if these values were experimentally confirmed. Also, the I_{sp} value of HT-7 reaches about 292 s, making it a very promising propellant component for use in future space explorations.

In order to experimentally validate the performance enhancement after doping of TAGP, HT-4 was selected for scaling up due to the better shape of the crystal and promising theoretical performance. Unfortunately, the scaling up brings about large inhomogeneity, which is the nature of the crystallization process with *in situ* 2D material doping. It was quite challenging to obtain homogeneous crystal density, and the average density of the obtained 50 g batch was about 1.94 g cm^{-3}. Modeling of the HT-4 powder and corresponding cylindrical pressed charges of the detonation velocity measurements are presented in Fig. S17.† Black spots can be clearly observed on the surfaces of the pressed charges, so that the pressed density is only 94% of the theoretical maximum density due to inhomogeneous doping. The measured VoD value for scaled HT-4 is about 9292 m s^{-1}, whereas it is 9158 m s^{-1} for pristine HMX under the same experimental conditions. Such results show possible further improvement of the performance *via* the use of better preparation techniques using this constraint doping strategy.

In summary, we demonstrated herein a new synthetic route to the *in situ* generation of TAGP in the presence of HMX molecules to modify and improve the performance of the resulting hybrid crystalline EMs. It is a facile and efficient approach that can be used to improve the energy density of nitramine crystals, resulting in the formation of fairly good 2D materials with reinforced crystal structures. More importantly, the dual-effect of constraining and doping of TAGP greatly increased the density of the resulting crystals, and hence the energetic performances were significantly improved, surpassing that of the most powerful energetic compound CL-20 currently used. We believe that the successful demonstration of this interesting "net-fishing" system in crystal engineering or materials science could somehow inspire more scientists to conceive better ideas for the construction of novel crystalline materials for use in various applications.

Author contributions

Q. L. Y. designed the proposal and outline of the research. X. X. Z. and Q. L. Y. performed the synthesis of the involved target materials, whereas J. Y. L. and W. H. carried out the SEM and XPS characterizations, both under the supervision of Q. L. Y. and P. J. L. In addition, Q. H. Z. and S. H. did the measurements of the density, FTIR, NMR and evaluation of the molecular structure. Moreover, Z. J. Y. participated in the performance tests of the involved materials, including detonation velocity and sensitivity analyses; X. X. Z. and F. D. N. performed the DSC/TG experiments; G. Q. H. carried out the combustion experiments. C. Y. Z did the theoretical calculations of the single crystal structure of qy-HMX. Q. L. Y. wrote the first draft of the manuscript with input from the rest of the authors. All the authors contributed to the final version.

Conflicts of interest

There are no conflicts to declare.

Acknowledgements

This work was supported by funding of National Defense Basic Science Foundation of China (Project No. 61407200204). We thank Mr D.-Y. Tang and Dr Shuwen Chen in our group for analyses of XPS spectra; Dr Z. Y. Zhang (Shanghai Institute of Materia Medica, Chinese Academy of Sciences) for testing of crystal structure and crystallographic analysis; additional data are in the ESI.†

References

1 Q. H. Zhang and J. M. Shreeve, Energetic Ionic Liquids as Explosives and Propellant Fuels: A New Journey of Ionic Liquid Chemistry, *Chem. Rev.*, 2014, **114**(20), 10527–10574.
2 W. He, P. J. Liu, G. Q. He, M. Gozin and Q. L. Yan, Highly Reactive Metastable Intermixed Composites (MICs): Preparations and Characterizations, *Adv. Mater.*, 2018, **30**(41), 1706293.
3 Y. Wang, Y. Liu, S. Song, Z. J. Yang, X. J. Qi, K. C. Wang, Y. Liu, Q. H. Zhang and Y. Tian, Accelerating the Discovery

of Insensitive High Energy-density Materials by a Materials Genome Approach, *Nat. Commun.*, 2018, **9**, 2444.

4 C. Zhang, C. G. Sun, B. C. Hu, C. M. Yu and M. Lu, Synthesis and Characterization of the Pentazolate Anion Cyclo-N_5^- in $(N_5)_6(H_3O)_3(NH_4)_4Cl$, *Science*, 2017, **355**, 374–376.

5 Y. G. Xu, Q. Wang, C. Shen, Q. H. Lin, P. C. Wang and M. Lu, A Series of Energetic Metal Pentazolate Hydrates, *Nature*, 2017, **549**, 78–81.

6 B. Tan, M. Huang, X. Long, J. Li, X. Yuan and R. Xu, From planes to cluster: The Design of Polynitrogen Molecules, *Int. J. Quantum Chem.*, 2015, **115**(2), 84–89.

7 Y. Li, J. Hao, H. Liu, S. Lu and J. S. Tse, High-energy Density and Super-hard Nitrogen-rich B-N Compounds, *Phys. Rev. Lett.*, 2015, **115**(10), 105502.

8 Q.-L. Yan, M. Gozin, F.-Q. Zhao, A. Cohen and S.-P. Pang, High Energetic Compositions Based on Functionalized Carbon Nanomaterials, *Nanoscale*, 2016, **8**, 4799–4851.

9 R. P. Dias and I. F. Silvera, Observation of the Wigner-Huntington Transition to Metallic Hydrogen, *Science*, 2017, **355**, 15–718.

10 M. J. Lipp, W. J. Evans, B. J. Baer and C.-S. Yoo, High-energy-density Extended CO solid, *Nat. Mater.*, 2005, **4**, 211–215.

11 Q.-L. Yan, F.-Q. Zhao, K. K. Kuo, X.-H. Zhang, S. Zeman and L. T. DeLuca, Catalytic Effects of Nano Additives on Decomposition and Combustion of RDX-, HMX-, and AP-Based Energetic Compositions, *Prog. Energy Combust. Sci.*, 2016, **57**, 75–136.

12 A. K. Nandi, M. Ghosh, V. B. Sutar and R. K. Pandey, Surface Coating of Cyclotetramethylenetetranitramine (HMX) crystals with the insensitive high explosive 1,3,5-triamino-2,4,6-trinitrobenzene (TATB), *Cent. Eur. J. Energ. Mater.*, 2012, **9**(2), 119–130.

13 Ø. H. Johansen, J. D. Kristiansen, R. Gjersøe, A. Berg, T. Halvorsen, K.-T. Smith and G. Nevstad, RDX and HMX with Reduced Sensitivity Towards Shock Initiation: RS-RDX and RS-HMX, *Propellants, Explos., Pyrotech.*, 2008, **33**, 20–24.

14 Q. Wang, X. Feng, S. Wang, N. Song, Y. Chen, W. Tong, Y. Han, L. Yang and B. Wang, Metal-Organic Framework Templated Synthesis of Copper Azide as the Primary Explosive with Low Electrostatic Sensitivity and Excellent Initiation Ability, *Adv. Mater.*, 2016, **28**, 5837.

15 O. Bolton and A. J. Matzger, Improved Stability and Smart-Material Functionality Realized in an Energetic Cocrystal, *Angew. Chem., Int. Ed.*, 2011, **50**, 8960–8963.

16 Q.-L. Yan, P.-J. Liu, A.-F. He, J.-K. Zhang, Y. Ma, H.-X. Hao, F.-Q. Zhao and M. Gozin, Photosensitive but Mechanically Insensitive Graphene Oxide-Carbohydrazide-Metal Hybrid Crystalline Energetic Nanomaterials, *Chem. Eng. J.*, 2018, **338**, 240–247.

17 W. He, B.-W. Tao, B. Z.-J. Yang, G. C. Yang, X. Guo, P.-J. Liu and Q.-L. Yan, Mussel-Inspired Polydopamine-directed Crystal Growth of Core-shell *n*-Al@PDA@CuO Metastable Intermixed Composites, *Chem. Eng. J.*, 2019, **369**, 1093–1101.

18 S.-W. Chen, W. He, C.-J. Luo, T. An, J. Chen, Y. Yang, P.-J. Liu and Q.-L. Yan, Thermal Behavior of Graphene Oxide and its Stabilization Effects on Transition Metal Complexes of Triaminoguanidine, *J. Hazard. Mater.*, 2019, **368**, 404–411.

19 W. He, P.-J. Liu, F.-Y. Gong, B. W. Tao, J. Gu, Z.-J. Yang and Q.-L. Yan, Tuning the Reactivity of Metastable Intermixed Composite *n*-Al/PTFE by Polydopamine Interfacial Control August, *ACS Appl. Mater. Interfaces*, 2018, **10**(38), 32849–32858.

20 F. Y. Gong, Z. Yang, W. Qian, Y. Liu, J. Zhang, L. Ding, C. Lin, C. Zeng and Q.-L. Yan, Kinetics for the Inhibited Polymorphic Transition of HMX Crystal after Strong Surface Confinement, *J. Phys. Chem. C*, 2019, **123**(17), 11011–11019.

21 Z. Yang, J. Li, B. Huang, S. Liu, Z. Huang and F. Nie, Preparation and Properties Study of Core-Shell CL-20/TATB Composites, *Propellants, Explos., Pyrotech.*, 2014, **39**, 51–58.

22 J.-Y. Lyu, S. Chen, W. He, X.-X. Zhang, D.-Y. Tang, P.-J. Liu and Q.-L. Yan, Fabrication of High-Performance Graphene Oxide doped PVDF/CuO/Al Nanocomposites *via* Electrospinning, *Chem. Eng. J.*, 2019, **368**, 129–137.

23 C.-S. Yoo and H. Cynn, Equation of state, Phase transition, Decomposition of β-HMX at High Pressures, *J. Chem. Phys.*, 1999, **111**(22), 10229–10235.

24 Q.-L. Yan, A. Cohen, A. K. Chinnam, N. Petrutik, A. Shlomovich, L. Burstein and M. Gozin, Layered 2D Triaminoguanidine-Glyoxal Polymer and Its Transition Metal Complexes, as Novel Insensitive Energetic Nanomaterials, *J. Mater. Chem. A*, 2016, **4**, 18401–18408.

25 T. Xu, Y. Xiong, F. Zhong, L. Wang, X. Hao and H. Wang, Chemical Transformation of HMX Induced by Low Energy Electron Beam Irradiation, *Propellants, Explos., Pyrotech.*, 2011, **36**(6), 499–504.

26 T. B. Brill and R. J. Karpowicz, Solid Phase Transition Kinetics: The Role of Intermolecular Forces in the Condensed-phase Decomposition of HMX, *J. Phys. Chem.*, 1982, **86**, 4260–4265.

27 D. A. Jacques and J. Trewhella, Small-angle scattering for structural biology-Expanding the frontier while avoiding the pitfalls, *Protein Sci.*, 2010, **19**(4), 642–657.

28 H. D. T. Mertens and D. I. Svergun, Structural characterization of proteins and complexes using small-angle X-ray solution scattering, *J. Struct. Biol.*, 2010, **172**(1), 128–141.

29 C. S. Choi and H. P. Boutin, *Acta Crystallogr., Sect. B: Struct. Crystallogr. Cryst. Chem.*, 1970, **26**, 1235.

